Single-nucleon transfer reactions on ^{18}F

A. S. Adekola,[1,*] C. R. Brune,[1] D. W. Bardayan,[2] J. C. Blackmon,[2,†] K. Y. Chae,[3,4] C. Domizioli,[3] U. Greife,[5] Z. Heinen,[1] M. J. Hornish,[1] K. L. Jones,[6,‡] R. L. Kozub,[7] R. J. Livesay,[4,§] Z. Ma,[3] T. N. Massey,[1] B. Moazen,[3] C. D. Nesaraja,[2] S. D. Pain,[6,‖] J. F. Shriner Jr.,[7] N. D. Smith,[7] M. S. Smith,[2] J. S. Thomas,[6,¶] D. W. Visser,[8] and A. V. Voinov[1]

[1]*Department of Physics and Astronomy, Ohio University, Athens, Ohio 45701, USA*
[2]*Physics Division, Oak Ridge National Laboratory, Oak Ridge, Tennessee 37831, USA*
[3]*Department of Physics and Astronomy, University of Tennessee, Knoxville, Tennessee 37996, USA*
[4]*Department of Physics, Sungkyunkwan University, Suwon 440-746, Korea*
[5]*Department of Physics, Colorado School of Mines, Golden, Colorado 80401, USA*
[6]*Department of Physics and Astronomy, Rutgers University, Piscataway, New Jersey 08854, USA*
[7]*Department of Physics, Tennessee Technological University, Cookeville, Tennessee, 38505, USA*
[8]*Department of Physics and Astronomy, University of North Carolina, Chapel Hill, North Carolina 27599, USA*

(Received 27 July 2011; published 17 November 2011)

Simultaneous measurement of the proton-transfer ^{18}F$(d,n)^{19}$Ne and neutron-transfer ^{18}F$(d,p)^{19}$F reactions were performed with a ^{18}F radioactive beam at the Holifield Radioactive Ion Beam Facility at Oak Ridge National Laboratory. The experiments clarify the nuclear structure of ^{19}Ne near the proton threshold, which is relevant for understanding the rates of proton-induced reactions on ^{18}F in novae. Analogs for several states in the mirror nucleus ^{19}F have not yet been identified in ^{19}Ne, indicating that the level structure of ^{19}Ne in this region is incomplete. We observed 15 levels in ^{19}Ne from the ^{18}F$(d,n)^{19}$Ne measurement and 18 levels in ^{19}F from the ^{18}F$(d,p)^{19}$F measurement. Angular distributions were extracted for all strongly populated states and compared to distorted-wave Born approximation calculations. The angular distributions for all the known states in the two nuclei determined in this work are consistent with their previously assigned spins and parities. The spectroscopic factors determined for these levels in the two nuclei are reported.

DOI: 10.1103/PhysRevC.84.054611 PACS number(s): 27.20.+n, 26.50.+x, 25.40.Hs, 25.40.Ny

I. INTRODUCTION

Precise determination of the rates of proton-induced reactions on the long-lived radioisotope ^{18}F is desirable to improve our understanding of the role that ^{18}F plays in annihilation γ-ray emission from novae and in possible heavier-element nucleosynthesis in x-ray bursts. At temperatures in the range of $(1–4)\times 10^8$ K, the rates of the ^{18}F$(p,\alpha)^{15}$O and ^{18}F$(p,\gamma)^{19}$Ne reactions depend critically on individual ^{19}Ne resonances around the proton threshold of 6411 keV [1]. Several measurements with different experimental techniques using stable and radioactive beams have been undertaken to search for excited states of ^{19}Ne and to determine their properties [2–10]. However, there remains considerable uncertainty in the level structure of ^{19}Ne, where as many as seven levels in the excitation energy range of interest of 6.4–7.4 MeV appear to be missing with respect to analog states of the corresponding mirror nucleus ^{19}F [9,11–14].

Neutron-transfer measurements to states in ^{19}F were recently used to determine neutron reduced widths, which can then be related to proton widths in ^{19}Ne via mirror symmetry. While these studies have contributed significantly to our understanding of the situation, there remains considerable uncertainty in the assignment of analog states between ^{19}F and ^{19}Ne [12,15]. Many of the observed states in ^{19}Ne do not have measured spins and parities but are assigned based on their putative analog states in ^{19}F. The properties of these unobserved states and precise determination of isospin-mirror symmetry between these two nuclei will influence the ^{18}F + p reaction rates.

In this paper, we describe simultaneous measurements of the proton-transfer and neutron-transfer reactions on ^{18}F to states in ^{19}Ne and ^{19}F, respectively. Transfer reactions induced by radioactive beams on deuterium targets are a powerful means for extracting nuclear structure information [15–19]. The spectroscopic information determined from these measurements comprises the excitation energies and the transferred angular momentum required to populate a given level in ^{19}Ne and ^{19}F. The angular distributions were compared to distorted-wave Born approximation (DWBA) calculations to extract spectroscopic factors for all the well-populated states in the two nuclei. The astrophysical implications of the ^{18}F(d,n) study have been presented in a Rapid Communication [20]. The present paper describes the simultaneous study of the ^{18}F(d,n) and ^{18}F(d,p) reactions, including details of

*aadekola@physics.rutgers.edu; Current address: Department of Physics and Astronomy, Rutgers University, Piscataway, New Jersey 08854, USA.
†Current address: Department of Physics and Astronomy, Louisiana State University, Baton Rouge, Louisiana 70803, USA.
‡Current address: Department of Physics and Astronomy, University of Tennessee, Knoxville, Tennessee 37996, USA.
§Current address: Oak Ridge National Laboratory, Oak Ridge, Tennessee 37831, USA.
‖Current address: Physics Division, Oak Ridge National Laboratory, Oak Ridge, Tennessee 37831, USA.
¶Current address: School of Electronics and Physical Sciences, University of Surrey, Guildford, Surrey GU2 7XH, United Kingdom.

the analysis, and presents information on observed analog states in ^{19}Ne and ^{19}F. The present experimental approach provides direct determination of spectroscopic strength and new constraints on their spin and parity for the observed levels in ^{19}Ne near the proton threshold and provides a multilevel spectroscopic application of the (d,n) reaction with a radioactive beam.

II. EXPERIMENT DETAILS

The ^{18}F beam was produced at the Oak Ridge National Laboratory's Holifield Radioactive Ion Beam Facility [21] using the Isotope Separator On-line (ISOL) technique. The driver accelerator, the Oak Ridge Isochronous Cyclotron (ORIC), provides $\sim$3 μA of 85-MeV α beam to a thick hafnium dioxide (HfO_2) target [22]. Atoms of ^{18}F were produced via the ^{16}O$(\alpha, pn)^{18}$F reaction. The HfO_2 target was in fibrous form ($\sim$4-μm diameter) and is heated for fast diffusion of ^{18}F atoms out of the target. The fluorine atoms produced diffuse through the target material and effuse through a transport line to the cesium ion source to be negatively ionized. The beam passes through two stages of mass separation before injection into a 25-MV tandem electrostatic accelerator with excellent beam quality of $\Delta E/E = 1 \times 10^{-4}$ [21]. In this experiment, the beam was stripped to charge state $q = 9^+$ before the analyzing magnet and was therefore isotopically pure.

A 716 μg/cm^2 CD_2 target was bombarded for $\sim$117 h with a 150-MeV ^{18}F beam with an intensity of $\sim 2.2 \times 10^6$/s. The thickness of the target was determined from the technique of energy loss in the target by known energy of an α particle from an α source. The beam energy of $E_{\text{c.m.}} = 14.9$ MeV was chosen because the reaction is well described by DWBA calculations at this energy and the heavier reaction products are kinematically focused forward in the laboratory with energies appropriate for particle identification with E-ΔE Si detectors. In this case, the neutrons (or protons) from the (d,n) [or (d,p)] reaction are predominantly emitted at backward angles while the ^{19}Ne (or ^{19}F) are limited to a narrow cone at forward angles. The ^{19}Ne ions of interest are highly excited and promptly decay into $\alpha + ^{15}$O nuclei. The same holds true for states in ^{19}F, which decay into $\alpha + ^{15}$N. These decay products were detected in coincidence in position-sensitive E-ΔE telescopes. The detection system (shown in Fig. 1) was made up of six telescopes and each consisted of a ΔE detector followed by an E detector, both of which are 5 × 5 cm. The ΔE detectors have 16 strips and are position sensitive while the rear detectors were pads that simply measured energy. The use of these detectors allowed for energy measurement as well as both position determination and particle identification. Two of the telescopes ("inner" with ΔE detectors of $\sim$62-μm thickness) covered laboratory angles of 2.5°–8.5° on either side of the beam axis (nominally 1.75–6.75 cm horizontal distance from the beam axis) and were optimized to measure heavier particles. The remaining four telescopes ("outer" with ΔE detectors of $\sim$144-μm thickness) covered laboratory angles of 10.5°–16.5° on either side of the beam axis (nominally 8.35–13.35 cm horizontal distance from the beam axis). They were optimized to detect the α particles.

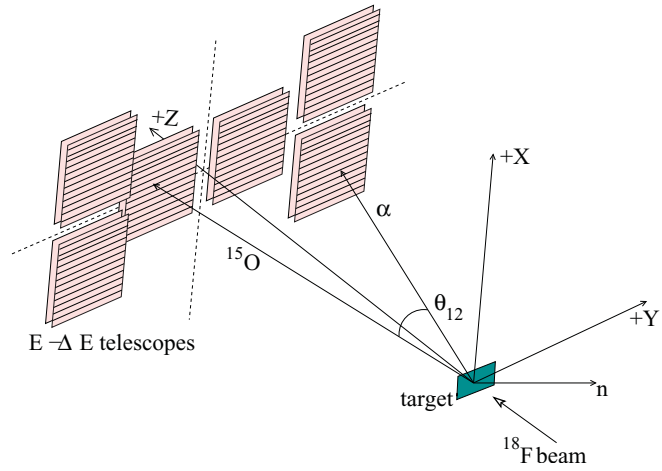

FIG. 1. (Color online) Schematic diagram of the six 5 × 5-cm E-ΔE detector telescopes employed for the measurement. The beam axis passes through the midpoint between the two inner telescopes.

Several additional measurements were undertaken to study backgrounds and for calibration purposes. The 150-MeV ^{18}F beam was also used to bombard a 630 μg/cm^2 CH_2 target to study the possibility of background reactions coming from hydrogen in the target (e.g., from water vapor or imperfect enrichment), as the (p,α) reaction on ^{18}F also yields $\alpha + ^{15}$O coincidences. The 150-MeV ^{18}F beam was also used to bombard a 1 mg/cm^2 ^{12}C foil to assess the possible role of background reactions coming from reactions on the carbon in the target. For calibration purposes we measured the elastic scattering of a 115-MeV ^{16}O beam from a 410 μg/cm^2 CD_2 target and the elastic scattering of 20-, 30- and 40-MeV α particles from a 500 μg/cm^2 gold target.

III. ANALYSIS AND RESULTS

A. Kinematics

Consider a three-body final state reaction which started with a beam particle B hitting a target T, resulting in the production of an excited or resonant particle A^* and a recoil particle 3 described as

$$B + T \rightarrow A^* + 3 \rightarrow (1 + 2) + 3. \tag{1}$$

Particle A^* sequentially decays into particles 1 and 2. The breakup energy of the intermediate state is given by the relative energy between particles 1 and 2 and is given to a good approximation by

$$E_{\text{rel}} = \frac{E_1 E_2 + m_1 E_2 + m_2 E_1}{m_1 + m_2} - \frac{\cos\theta_{12}\sqrt{E_1^2 + 2m_1E_1}\sqrt{E_2^2 + 2m_2E_2}}{m_1 + m_2}, \tag{2}$$

where E_1, m_1 and E_2, m_2 are the kinetic energies and rest masses of the decay products and θ_{12} is the laboratory angle between them.

By detecting the energy and position of the charged particles, their momenta and hence the excitation energy of

the decaying state in ^{19}Ne (or ^{19}F) relative to the $\alpha + {}^{15}$O (or $\alpha + {}^{15}$N) threshold ("relative energy") can be calculated using

$$E_x = E_{\rm th} + E_{\rm rel}, \tag{3}$$

where $E_{\rm th}$ is the threshold energy for the decay process. For $^{19}\text{Ne} \rightarrow \alpha + {}^{15}\text{O}$, $E_{\rm th} = 3529$ keV, and for $^{19}\text{F} \rightarrow \alpha + {}^{15}\text{N}$, $E_{\rm th} = 4014$ keV. The total energy of the reaction process is calculated from

$$E_{\rm tot} = E_1 + E_2 + E_3, \tag{4}$$

where E_3 is the energy of the undetected recoil particle determined from conservation of momentum. Thus, the three-body reaction Q value can be obtained using

$$Q = E_1 + E_2 + E_3 - E_b, \tag{5}$$

where E_b is the beam energy.

B. Background reactions and analysis of Q values

Particle identification plots are shown in Fig. 2. Complete isotopic separation is observed for H and He while there is complete Z separation and partial isotopic separation for the heavier nuclei. The $\alpha + {}^{15}$O (or $\alpha + {}^{15}$N) coincidence requirement was very effective for reducing backgrounds in this experiment. However, in order to eliminate backgrounds that give true $\alpha + {}^{15}$O (or $\alpha + {}^{15}$N) coincidences, we have found it useful to calculate two Q values for each event, with one of them being the reaction of interest, and plotting them as a two-dimensional histogram.

For $\alpha + {}^{15}$O coincidences, we have calculated Q_0 assuming the reaction of interest $^2\text{H}(^{18}\text{F}, \alpha + {}^{15}\text{O})n$ and Q_1 assuming a two-body final-state reaction $^1\text{H}(^{18}\text{F}, \alpha)^{15}\text{O}$. The resulting two-dimensional Q_1 versus Q_0 histogram is shown in Fig. 3(a). This spectrum is useful for both identifying the reaction of interest and determining which background reactions are present. A projection to the Q_0 axis reveals two peaks, as shown in Fig. 3(b). Peak 1 was measured at $Q_0 = 0.665(14)$ MeV and it corresponds to true $\alpha + {}^{15}$O events of interest, which is in agreement with the calculated Q value of 0.654 MeV for the $^2\text{H}(^{18}\text{F}, \alpha + {}^{15}\text{O})n$ reaction. Peak 2 was

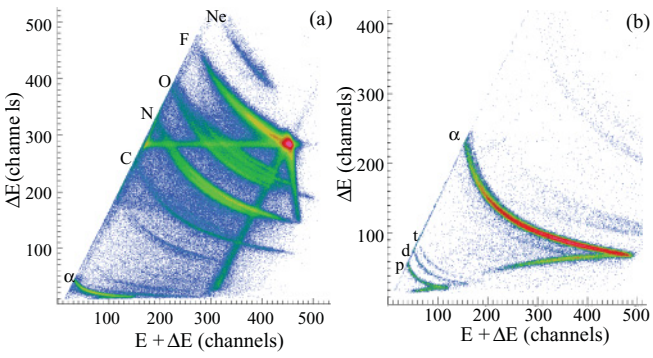

FIG. 2. (Color online) The $E_{\rm tot}$-ΔE spectrum from the experiment for the inner detector (a) and the outer detector (b). The loci of nuclei detected by the detectors are indicated. There was complete isotopic separation for H and He and complete Z separation but partial isotopic separation for heavier nuclei.

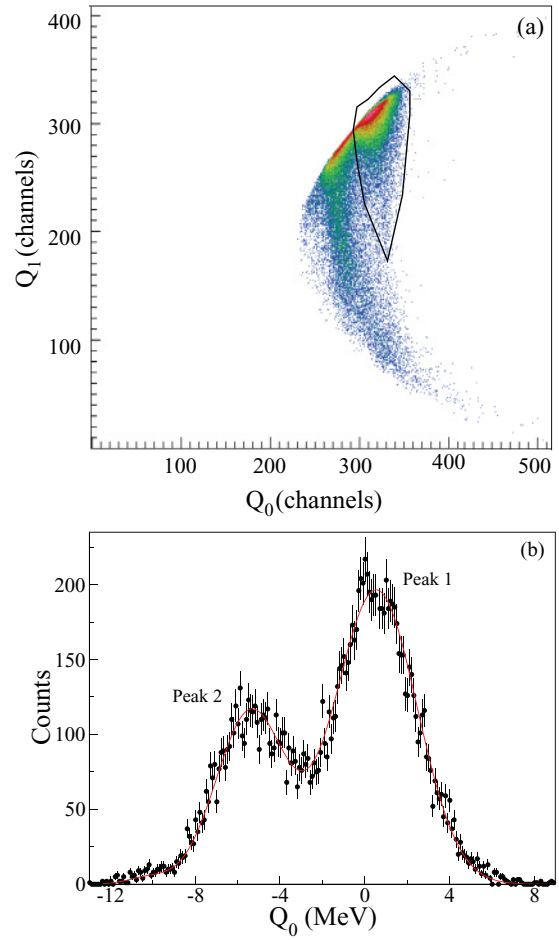

FIG. 3. (Color online) (a) The two-dimensional Q-value spectrum for $\alpha + {}^{15}$O. Q_0 assumes $^2\text{H}(^{18}\text{F}, \alpha + {}^{15}\text{O})n$ while Q_1 assumes $^1\text{H}(^{18}\text{F}, \alpha)^{15}\text{O}$. (b) The projection of the two-dimensional plot to the Q_0 axis.

measured at $Q_0 = -5.141(20)$ MeV and it corresponds to events due to reactions leading to bound excited states of ^{15}O with Q_0 reduced by the energy equivalent to the energy of the photon emitted by $^{15}\text{O}^*$ to go to the ground state. More details about this technique are available in Ref. [23].

The same procedure was utilized to analyze the $\alpha + {}^{15}$N coincidences. Here for Q_0 the reaction of interest is assumed to be $^2\text{H}(^{18}\text{F}, \alpha + {}^{15}\text{N})p$ and for Q_1 the possibility of the ^{18}F breakup reaction $^{12}\text{C}(^{18}\text{F}, \alpha + {}^{14}\text{N})^{12}\text{C}$ is assumed. The measured Q value of 4.325(22) MeV, which corresponds to true $\alpha + {}^{15}$N events of interest, compares reasonably with the calculated Q value of 4.194 MeV for the reaction.

By utilizing a two-dimensional gate on the reaction of interest, the background in the relative energy spectra was found to be greatly reduced. The solid curve in Fig. 3(a) shows the gate used to select $^2\text{H}(^{18}\text{F}, \alpha + {}^{15}\text{O})n$ events for subsequent analysis. A band of events is seen to curve into the "good" Q_0 range for low values of Q_1. The events inside these bands and with correct Q_0 are from the decay of ^{19}Ne with large $\theta_{\rm c.m.}$. The angular range of interest is $\theta_{\rm c.m.} \leqslant 50^\circ$, suggesting that the events with large $\theta_{\rm c.m.}$ are from the background. For this reason, the gate efficiency is essentially 100%.

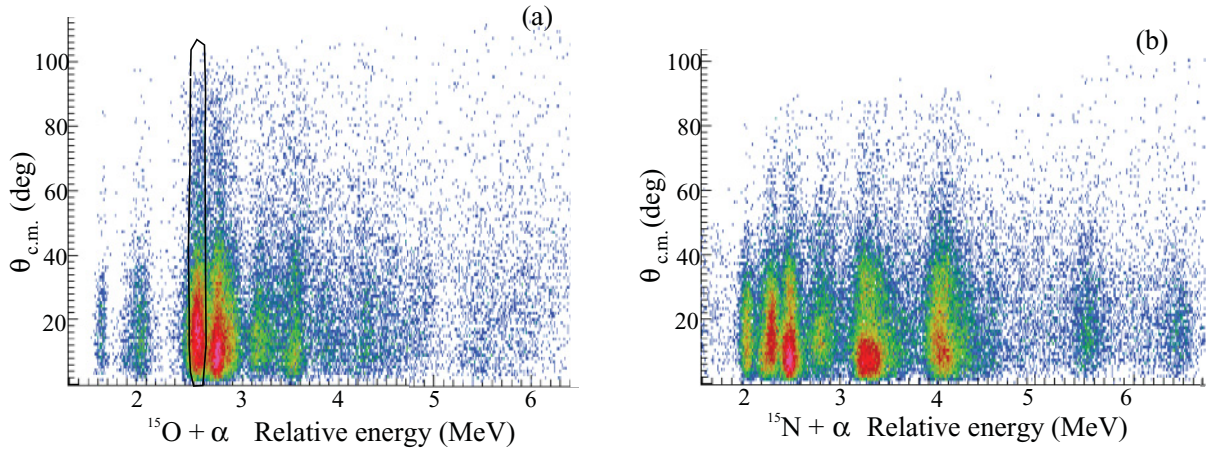

FIG. 4. (Color online) The two-dimensional plots of neutron $\theta_{\text{c.m.}}$ vs $\alpha + {}^{15}\text{O}$ (a) and proton $\theta_{\text{c.m.}}$ vs $\alpha + {}^{15}\text{N}$ (b) relative energy revealing observed states in ^{19}Ne and ^{19}F, respectively. As an example, the closed line in (a) is the gate used to extract the angular distribution for that state.

C. Relative energy and angular distribution

The momentum vector of the undetected neutron or proton was deduced via momentum conservation, which allows the angular distribution of a given final state to be reconstructed. Figure 4(a) shows two-dimensional plots of neutron angle $\theta_{\text{c.m.}}$ versus $\alpha + {}^{15}\text{O}$ relative energy (in MeV), revealing states populated in ^{19}Ne. A similar plot is shown in Fig. 4(b) for proton angle $\theta_{\text{c.m.}}$ against $\alpha + {}^{15}\text{N}$ relative energy, showing states populated in ^{19}F.

1. Relative energy

The reconstructed relative energy spectra of $\alpha + {}^{15}\text{N}$ and $\alpha + {}^{15}\text{O}$ coincidences obtained using the same position and energy calibrations after Q-value gating are shown in Fig. 5. The relative energies were fitted with the MINUIT [24] package using the method of χ^2 minimization for the sum of Gaussian functions:

$$y_c = \sum_i \frac{A_i}{\sqrt{2\pi w_i^2}} \exp\left(-\frac{(E_{\text{rel}} - [E_r]_i)^2}{2w_i^2}\right). \quad (6)$$

Equation (6) represents the sum over i peaks, where y_c is the number of counts as a function of relative energy, and the variables A, E_r, and w represent the area, resonance energy, and width of each peak, respectively. Normally, these are all free parameters. However, in the case of unresolved peaks, the variable w was constrained to be the same for all peaks. The excitation energies were determined using Eq. (3) with the appropriate threshold energy.

2. States in ^{19}F

The observed excitation energies of ^{19}F are labeled in Fig. 5(a) and listed in Table I along with the results from the $^{18}\text{F}(d,p)$ experiments of Kozub *et al.* [12] and de Sèrèville *et al.* [25,26].

The experiment of Kozub *et al.* was performed at a somewhat lower energy than the present one ($E_{\text{c.m.}} = 10.88$ MeV versus 14.94 MeV). We see all of the states reported by Kozub *et al.* for $E_x > 6$ MeV. The non observation of the low-lying states is expected as the present experiment is only capable of measuring states with $E_{\text{rel}} > 1.5$ MeV ($E_x > 5.5$ MeV). It is interesting to note that both experiments see high-lying states at $E_x = 9.58$ and 10.54 MeV. It is somewhat surprising that Kozub *et al.* did not see the level we observe at $E_x = 6.33$ MeV. There is a structure visible in their proton singles spectrum at an energy corresponding to this state; perhaps the ^{15}N particles from the decay of that state did not receive a large enough kick to be efficiently detected by the forward annular silicon strip detector used in that experiment.

In their $^{18}\text{F}(d,p)$ experiment, de Serèville *et al.* [25,26] observed particle groups corresponding to levels in ^{19}F at $E_x = 6.1$, 6.3, 6.5, 6.8, and 7.3 MeV, which are also seen in the present experiment.

3. States in ^{19}Ne

Excitation energies of levels in ^{19}Ne from the present work are labeled in Fig. 5(b) and listed in Table II along with those taken from the compilations of Nesaraja *et al.* [13] and Tilley *et al.* [27]. Our results for levels below $E_x < 7.834$ agree well with previous studies. Above this energy, the states become more broad and breakup into the $^{18}\text{F} + p$ channel becomes stronger. The result is that centroid extraction becomes more difficult above this energy, and it is difficult to establish a correspondence with known levels.

4. Angular distributions

To extract angular distributions for a populated level, gates have been drawn [an example of which is shown in Fig. 4(a)] on events within a given relative energy range. The number of counts in an angular bin was then extracted for each level. Each bin was 1° wide, except for the 0° bin, which is 0.5° wide. In

TABLE I. Observed excitation energies in ^{19}F and spectroscopic strengths for the strongly populated states compared with some previous work. The numbers in parentheses are the statistical uncertainties.

Present work					^{18}F$(d,p)^{19}$F[a]				^{18}F$(d,p)^{19}$F[b]				$2J^{\pi}$[c]
E_x	ℓ	$(2J+1)S_n$			E_x	S_n			E_x	S_n			
(keV)		$2s_{1/2}$	$1p_{1/2}$	$1d_{5/2}$	(keV)	$2s_{1/2}$	$1p_{1/2}$	$1d_{5/2}$	(keV)	$2s_{1/2}$	$1p_{1/2}$	$1d_{5/2}$	
5503(9)													
5780(30)													
6091(3)	2			0.88(2)					6.1[d]				
6331(2)	2			1.95(3)					6.3[e]				
6523(2)	0,2	0.64(2)		0.55(3)	6497(10)	0.11(4)		0.12(2)	6497/6528	0.2		0.2	3^+
6851(7)	1		0.37(2)		6794(11)		0.05(1)						3^-
7259(4)									7262				3^+
7358(7)	0,2	0.67(2)		0.06(1)	7306(10)[f]	0.16(3)		0.065(65)	7364				1^+
7669(40)													
8052(4)[g]	0,2	0.75(3)		0.41(2)	8040/8100	0.32(6)		0.15(3)					5^+,1^+
8236(26)													
8573(7)													
8878(8)													
9182(10)													
9566(6)	2			0.11(3)	9580(20)								
10174(32)													
10480(8)	2			0.41(2)	10540(20)								
11062(22)													

[a]References [12,15].
[b]References [25,28].
[c]Taken from Refs. [12,15].
[d]This consists of 6070- and 6088-keV states.
[e]This consists of 6255-, 6282-, and 6330-keV states.
[f]This is composed of known but unresolved states at 7262 and 7364 keV with $J^{\pi} = 3/2^+$ and $1/2^+$, respectively.
[g]This consists of known states at 8014 and 8138 keV.

order to correct the angular distribution for the gate efficiency, the distributions were renormalized such that the total number of counts in each distribution is equal to the number of counts determined for that state in the relative energy spectrum. The angular distributions were then converted to experimental differential cross sections according to the following equation:

$$\frac{d\sigma}{d\Omega} = \frac{N(E)}{\mathrm{In}\Delta\Omega(\theta_{\mathrm{c.m.}})\epsilon(\theta_{\mathrm{c.m.}})}, \tag{7}$$

where $N(E)$ is the number of α particles detected in coincidence with ^{15}O (or ^{15}N) for each resonance state in ^{19}Ne (or ^{19}F), I is the number of ^{18}F ions incident on the target, n is the number of deuterium atoms per unit area, $\Delta\Omega(\theta_{\mathrm{c.m.}})$ is the solid angle per bin of the differential cross section, and $\epsilon(\theta_{\mathrm{c.m.}})$ is the coincidence efficiency calculated as a function of center-of-mass angle for each excitation energy with our Monte Carlo simulation assuming that the decay is isotropic in the center-of-mass system. Each set of simulations has events generated with neutrons (or protons) emitted on a cone of constant θ. These simulations allow us to check the resolution in the reconstructed neutron (or proton) $\theta_{\mathrm{c.m.}}$. The width of the distribution (FWHM) varied from 2.5° near $\theta_{\mathrm{c.m}} = 0°$ up to 8° near $\theta_{\mathrm{c.m.}} = 40°$. The theoretical angular distributions shown below have been convolved with this experimental angular resolution.

5. *Monte Carlo simulations*

The experimental setup was originally designed with the aid of a Monte Carlo program which took into account the reaction kinematics as well as energy loss, energy and angle straggling, estimates for detector energy and position resolutions, and a finite beam spot. After the experiment, the program was updated with the measured parameters of the experiment, i.e., the target thickness, the detector geometry, and position and energy resolutions of the detectors. The simulations, in which center-of-mass isotropy for the breakup of ^{19}Ne (or ^{19}F) into $\alpha + {}^{15}$O (or $\alpha + {}^{15}$N) particles was assumed, have been very useful for checking various steps in the analysis and are also necessary to determine the efficiency, which is in turn needed to extract the cross sections. The resulting $\alpha + {}^{15}$O coincidence efficiency, integrated over the acceptance of our experiment, is shown as a function of E_{rel} in Fig. 6. The shape of the angular distribution was assumed to be given by an $\ell_p = 0$ DWBA calculation. The efficiency peaks near $E_{\mathrm{rel}} = 3$ MeV as a result of the optimization of the geometry for observing states near the proton threshold in ^{19}Ne. This efficiency curve also explains qualitatively the observed low-energy and high-energy fall-offs in the measured relative energy spectra (see Fig. 5).

Figure 7 shows the calculated FWHM resolution of the reconstructed E_{rel} as a function of E_{rel}. Additionally, the

measured experimental resolution of strongly populated and isolated states from this study is shown in Fig. 7. The calculated resolution is seen to be in reasonably good agreement with the measured experimental resolution. Note that the measured width can exceed the experimental resolution if the intrinsic width of the state is large, or if the peak consists of two or more unresolved states.

D. DWBA calculations

In order to deduce the orbital angular momentum of the transferred proton (or neutron) and to extract spectroscopic factors, a DWBA analysis of the neutron (or proton) angular distributions was performed with the code DWUCK4 [29]. We performed a similar analysis on the angular distributions extracted for the bound states using the code FRESCO [30]. The calculated differential cross sections and radial form factors obtained using FRESCO and DWUCK4 are in good agreement even though the calculations are performed using a finite- and zero-range interaction, respectively. The optical potentials for the incoming and outgoing channels presented in Table III are taken from Barrows *et al.* [31] and Perey and Perey [32], respectively. The potentials for the bound state was chosen to be Woods-Saxon in shape with the same radius and diffuseness as those of outgoing channels. This allows for the calculation of the proton width for a pure single-particle state Γ_{sp} using the technique of Vincent and Fortune [33], which has been incorporated into the DWUCK4 code. This quantity is needed to estimate the proton partial width Γ_p for states in ^{19}Ne above the proton threshold.

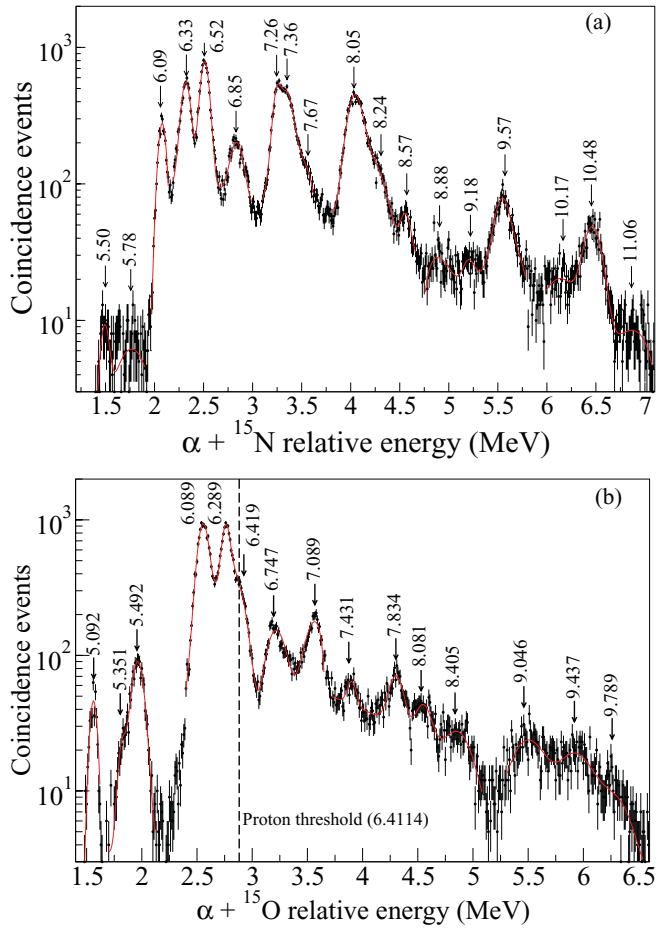

FIG. 5. (Color online) The relative energy spectra for $\alpha + {}^{15}$N (a) and $\alpha + {}^{15}$O (b) coincidences leading to excited states in ^{19}F and ^{19}Ne, respectively. The dots are experimental data and the red curves are the MINUIT fit. The corresponding excitation energies (in units of MeV) are written against the peaks.

TABLE II. Observed excitation energies in ^{19}Ne and spectroscopic strengths for the strongly populated states. The numbers in parentheses are the statistical uncertainties.

Present work					
E_x (keV)	ℓ	$(2J+1)S_p$			E_x (keV)[a]
		$2s_{1/2}$	$1p_{1/2}$	$1d_{5/2}$	
5092(3)	2			0.47(3)	5092(6)
5351(9)	0,2	0.02(4)		0.03(7)	5351(10)
5492(5)	2			0.38(2)	5463(20)
6089(2)	2			2.36(3)	6092(8)
6289(2)	0,2	0.92(3)		0.52(3)	6288(7)
6421(6)	1		0.50(2)		6419(6)
6747(5)	1		0.56(2)		6741(6)
7089(5)	0	1.46(5)			7076(16)
7431(8)					7420(14)
7834(6)					
8081(10)					
8405(16)					
9046(9)					
9437(11)					
9788(13)					

[a]References [13,27].

The theoretical differential cross section extracted from DWUCK4 is defined as

$$\left(\frac{d\sigma}{d\Omega}\right)_{\text{theory}} = N\frac{(2J+1)}{2J_i+1}\frac{1}{2j+1}\left(\frac{d\sigma}{d\Omega}\right)_{\text{DWK}}, \qquad (8)$$

where J_i and J are the spin of ^{18}F and the final states, respectively, $j = \ell \pm 1/2$ is the spin of the transferred nucleon, ℓ is the angular momentum transfer, the last quantity in Eq. (8)

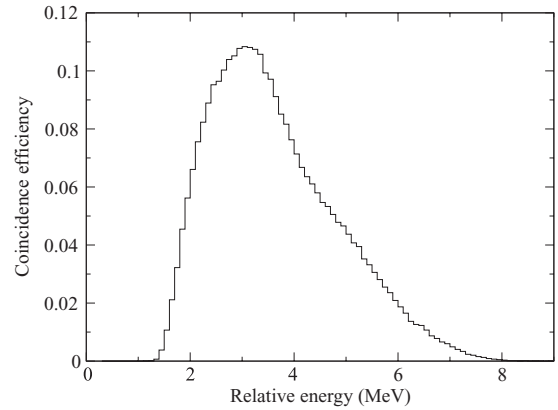

FIG. 6. The calculated coincidence efficiency for our geometry.

TABLE III. Optical potential parameters used in the DWBA analysis for the ^{18}F$(d,n)^{19}$Ne and ^{18}F$(d,p)^{19}$F reactions (with depths in MeV and lengths in femtometers).

Channel	V_0	r_0	a_0	W	r_W	a_W	$4W_D$	r_D	a_D	$V_{s.o.}$	$r_{s.o.}$	$a_{s.o.}$
^{18}F + d entrance	109.0	1.35	0.70	–	–	–	58.8	1.39	0.60	–	–	–
^{19}Ne + n exit	54.90	1.17	0.75	0.27	1.26	0.58	46.19	1.26	0.58	6.2	1.01	0.75
^{19}F + p exit	53.95	1.17	0.75	–	–	–	41.39	1.32	0.55	6.2	1.01	0.75

is the calculated value from the code DWUCK4, and $N = 1.55$ for the (d,n) and (d,p) reactions [29].

In the Monte Carlo simulation it is assumed that the breakup of ^{19}Ne and ^{19}F are isotropic in the center-of-mass system. Angular correlations for ^{18}F$(d,n)^{19}$Ne $\rightarrow {}^{15}$O + α and ^{18}F$(d,p)^{19}$F $\rightarrow {}^{15}$N + α have been calculated from scattering amplitudes produced with the code FRESCO [30]. The details of this procedure are given in the Appendix. We find for the important cases of pure ℓ_p and $\ell_n = 0$ transfer that the correlations vanish identically and the breakup is exactly isotropic. Correlations also vanish exactly for the breakup of $J = 1/2$ states in ^{19}Ne and ^{19}F. For the remaining cases, the correlations are found to be nonzero but are generally small (<20% deviation from isotropy). In a few cases larger deviations are seen for certain breakup angles (for example, for an $\ell_p = 2$ transfer to a $J^\pi = 5/2^+$ state), but after averaging over the detector acceptance we find these effects to be <15% for all cases.

E. Spectroscopic factors

Determination of the spectroscopic factors provides quantitative information about the single-particle structure of nuclei in the shell model. Knowledge of spectroscopic factors is also essential in estimating proton widths and asymptotic normalization coefficients, which are used in estimating astrophysical proton-capture rates. Spectroscopic factors were extracted by comparison of experimental angular distributions

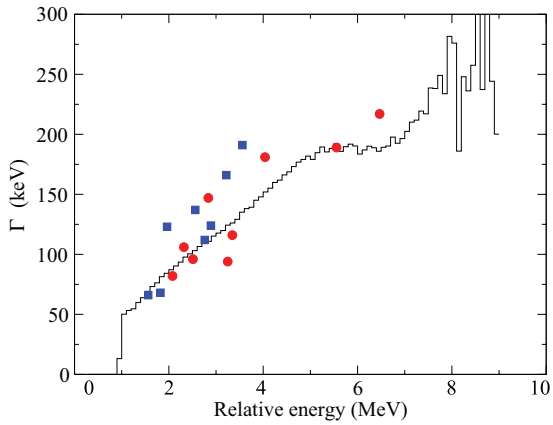

FIG. 7. (Color online) The calculated FWHM resolution for the reconstructed relative energy (solid curve) using our Monte Carlo simulations assuming $\alpha + {}^{15}$O. Some observed experimental resolutions are indicated for $\alpha + {}^{15}$O (squares) and $\alpha + {}^{15}$N (circles).

with the results of DWBA calculations using

$$\left(\frac{d\sigma}{d\Omega}\right)_{\rm exp} = \sum_i S_i \left[\left(\frac{d\sigma}{d\Omega}\right)_i\right]_{\rm theory}. \quad (9)$$

The coupling of $j = 1/2$ for the transferred proton or neutron with the ground-state spin of ^{18}F$(J^\pi = 1^+)$ allowed for more than one angular momentum transfer for a given final state in ^{19}Ne (or ^{19}F). For instance, the final-state wave function for proton capture by ^{18}F$(J_i^\pi = 1^+)$ to the ^{19}Ne$(J^\pi = 3/2^+)$ state can be described by

$$\psi_{3/2^+} = \beta[^{18}\mathrm{F}_{g.s} \otimes \pi_{2s_{1/2}}] + \gamma[^{18}\mathrm{F}_{g.s} \otimes \pi_{1d_{5/2}}] + \ldots, \quad (10)$$

where β and γ are the spectroscopic amplitudes of the s-wave and d-wave components, respectively. The shapes of the measured angular distributions strongly depend on the ℓ-transfer values. Determination of ℓ for the observed states in ^{19}Ne (or ^{19}F) requires a DWBA calculation with different values of ℓ, and then a comparison with the experimental angular distribution. In certain situations, the observed angular distribution cannot be described by a single angular momentum transfer and mixing must be considered, as indicated in Eq. (10). The transferred angular momentum was determined for all states where the statistics allowed a reasonable comparison with the results of the calculations.

Determination of the spin for the final states in ^{19}Ne (or ^{19}F) is still somewhat ambiguous. For instance, an $\ell = 0$ transfer would lead to assignment of spin-parity $1/2^+$ or $3/2^+$ to the final state in ^{19}Ne (or ^{19}F). Similarly, for $\ell = 1$ or 2 transfers, it is difficult to differentiate between $\ell + 1/2$ and $\ell - 1/2$ transitions. For this reason, the spin of the observed final states could not be determined solely from this work.

F. Error analysis

We have estimated systematic uncertainties on relative energies, differential cross sections, and the spectroscopic factors reported in this paper. Some sources of uncertainties and their associated contribution to these quantities are presented in Table IV. A systematic error of ±10 keV is estimated on the relative energies. The main sources of error come from the energy and position calibrations and those associated with the detectors' distances. The systematic error associated with the experimental differential cross section has been estimated to be 12%. The sources and percentage contributions to this error are listed in Table IV. In addition, the procedure for the extraction of angular distribution as described in Sec. III C 4, introduced a varied systematic error of 0–4%, depending on

TABLE IV. Systematic errors on some important quantities in this work.

Sources of error	Error
Relative energy	±10 keV
Differential cross section	
Number of deuterium nuclei in target	10.0%
Total number of ^{18}F ions on target	6.0%
Efficiency of Monte Carlo simulation and fit	2.0%
Beam spot size	1.8%
Beam spot position	0.5%
Differential cross section overall error	12.0%
Spectroscopic factor (DWBA)	
Differential cross section	12.0%
DWUCK and FRESCO difference	3.0%
Deuterium optical potential	15.0%
Proton/neutron optical potential	5.0%
Bound state potential	12.0%
Model	18.0%
Spectroscopic factor (DWBA)	30.0%

whether or not the state is isolated. The systematic uncertainty in spectroscopic factor is estimated to be 30%. The largest contribution to this error is essentially associated with the optical potentials. The sources and percentage contributions to this error are listed in Table IV.

IV. DISCUSSION

A. ^{18}F$(d,p)^{19}$F

The proton angular distributions for the (d,p) transfer to various states in ^{19}F are shown in Fig. 8. Additionally, the results of DWBA calculations using DWUCK4 are shown in Fig. 8. The ℓ transfer determined for all the levels in ^{19}F are presented in Table I. They were found to be consistent with the previously determined spins and parities. The spectroscopic factors were determined for states where the statistics allowed a reasonable comparison with DWBA calculations. Neutron spectroscopic factors extracted for these states are summarized in Table I, along with the results from the ^{18}F(d,p) experiments of Kozub *et al.* [12] and de Sèrèville *et al.* [25,26]. The spectroscopic factors are in reasonable agreement with previous studies.

B. ^{18}F$(d,n)^{19}$Ne

The neutron angular distributions for the (d,n) transfer to various states in ^{19}Ne are shown in Fig. 9. We extracted spectroscopic factors for levels at $E_x = 6089$, 6289, 6419, 6747, and 7089 keV where the statistics allowed a reasonable comparison with the results of DWBA calculations. The ℓ transfer determined for these levels and their corresponding spectroscopic factors are presented in Table II. The estimated partial proton widths of the states above the proton threshold

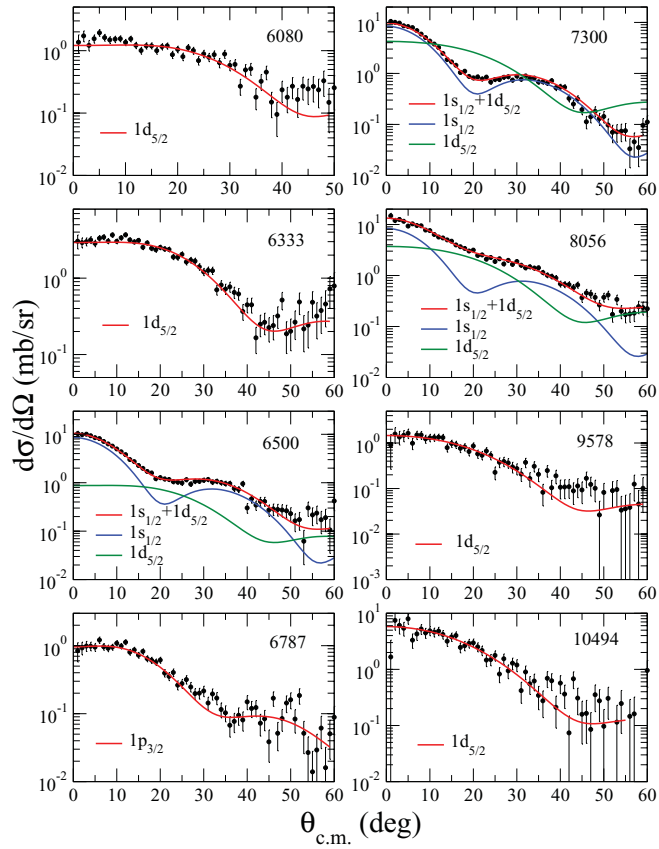

FIG. 8. (Color online) The differential cross section for the ^{18}F$(d,p)^{19}$F reaction to various final states. The curves were obtained from DWBA calculations with the set of optical potentials in Table III. The calculations have been scaled to the data with the spectroscopic factors determined in this work. All excitation energies are shown in keV.

presented in Table V were obtained using the relation [34]

$$\Gamma_p = S_p \Gamma_{\rm sp}, \tag{11}$$

where $\Gamma_{\rm sp}$ is the calculated proton width for a pure single-particle state and S_p is the spectroscopic factor.

1. 5091-, 5351-, and 5485-keV levels

The angular momentum transfer determined for levels at $E_x = 5091$, 5351, and 5485 keV are consistent with their known spin and parity.

2. 6741- and 7076-keV levels

The angular momentum transfer of 1 and 0, determined for levels at $E_x = 6741$ and 7076 keV, respectively, support their known spin and parity assignments. Proton widths of 7.3(6) eV and 13.5(7) keV were determined for the 6741-keV and 7076-keV states, respectively. The result for the 7076-keV state agrees well with the previously determined Γ_p of 15.2(1.0) keV [35]. For the 6741-keV state, our result is significantly larger than the previously determined value of 2.22(69) eV [11]. We note that the experimental uncertainty

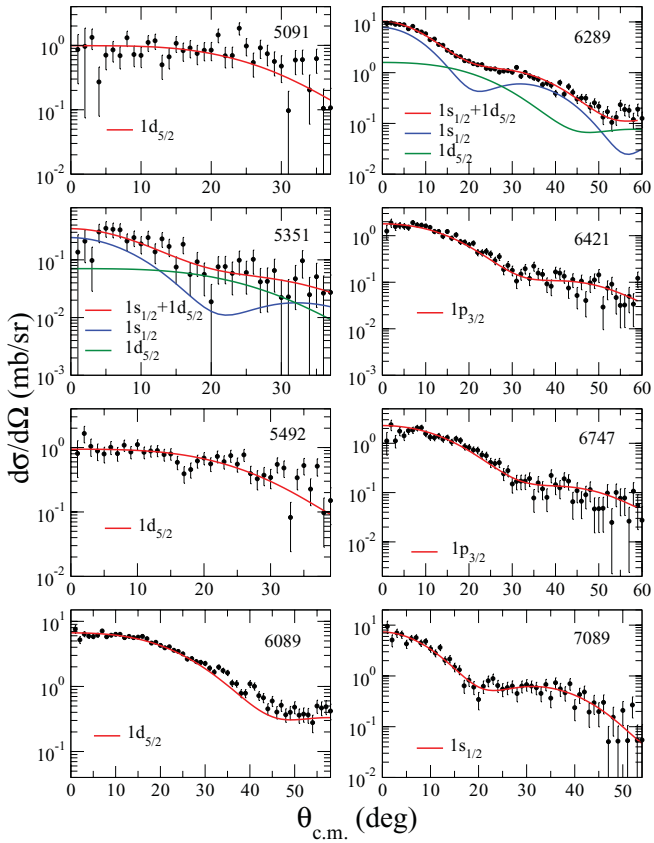

FIG. 9. (Color online) The differential cross section for the ^{18}F$(d,n)^{19}$Ne reaction to various final states. The curves were obtained from DWBA calculations with the set of optical potentials in Table III. The calculations have been scaled to the data with the spectroscopic factors determined in this work. All excitation energies are shown in keV.

was large in the previous result and contributions from nearby levels cannot be ruled out in the present work.

3. 6419- and 6449-keV levels

In the calculation of the ^{18}F$(p,\alpha)^{15}$O reaction rate, the levels at $E_x = 6419$ and 6449 keV (corresponding to resonance energies of $E_r = 8$ and 38 keV, respectively) are believed to be relevant. We observed the 6419-keV level but see no evidence of the 6449-keV level in our data. The angular distribution of the 6419-keV level indicates that the state is populated via transfer to the $1p$ orbital, in contrast to the value of $\ell = 0$ assumed previously [13] for the state. The J^π value of this state could be $1/2^-$ or $3/2^-$. The Γ_p value determined for this state is $2.54(8) \times 10^{-38}$ or $1.27(4) \times 10^{-38}$ keV for a $J^\pi = 1/2^-$ or $3/2^-$ assignment, respectively. This measurements also allow us to set an upper limit on Γ_p of the 38-keV resonance. Considering the fact that the 6419- and 6449-keV levels are 30 keV apart, we cannot completely eliminate the possibility of the 6449-keV level in our data. Instead of using one Gaussian function, we have used two Gaussian functions in the relevant energy region, as shown in Fig. 10, but constrained the peak centroids to take their corresponding relative energies.

TABLE V. Proton partial widths (in keV) for states above the proton threshold in ^{19}Ne from our measurement and comparison with some previous work. The numbers in parentheses are the statistical errors.

E_x (keV)	J^π	Present work	Ref. [13]
6419	$3/2^-$	$1.27(4) \times 10^{-38}$	$2.2(4) \times 10^{-37}$[a]
	$1/2^-$	$2.54(4) \times 10^{-38}$	–
6449	$3/2^+$	$\leqslant 2.35(4) \times 10^{-15}$	$4.0(4.0) \times 10^{-15}$
6741	$3/2^-$	$7.3(6) \times 10^{-3}$	$2.22(68) \times 10^{-3}$
7076	$3/2^+$	13.5(7)	15.2(1.0)

[a]This value is from previous works that assumed $J^\pi = 3/2^+$.

Allowing for a second Gaussian in the fitting with a centroid fixed at the known value, we find the following upper limits for the 6449-keV state: $S_p \leqslant 0.028$, corresponding to $\Gamma_p \leqslant 2.35 \times 10^{-15}$ keV for a $J^\pi = 3/2^+$ assignment.

4. 6289-keV level

The angular distribution of the subthreshold ^{19}Ne (6289-keV) state is well reproduced by $\ell = 0$ transfer with a small $\ell = 2$ admixture. The significant $\ell = 0$ strength in this state makes it relevant for the ^{18}F $+ p$ system. Two possible J^π values for the final state in ^{19}Ne (6289 keV) are $1/2^+$ (via proton transferred to the $2s_{1/2}$ or/and $1d_{3/2}$) or $3/2^+$ (via proton transferred to the $2s_{1/2}$ or/and $1d_{5/2}$ or/and $1d_{3/2}$), making it a likely mirror candidate for one of the three states in ^{19}F at $E_x = 6255$ keV ($1/2^+$), 6497 keV ($3/2^+$), and 6528 keV ($3/2^+$). The discovery of $\ell_p = 0$ for the subthreshold state in this measurement is consistent with the recent theoretical prediction of an s-wave state below the proton separation energy [36].

For bound states, the asymptotic normalization coefficient C_p is related to the spectroscopic factor via

$$C_p^2 = S_p C_{\rm sp}^2, \tag{12}$$

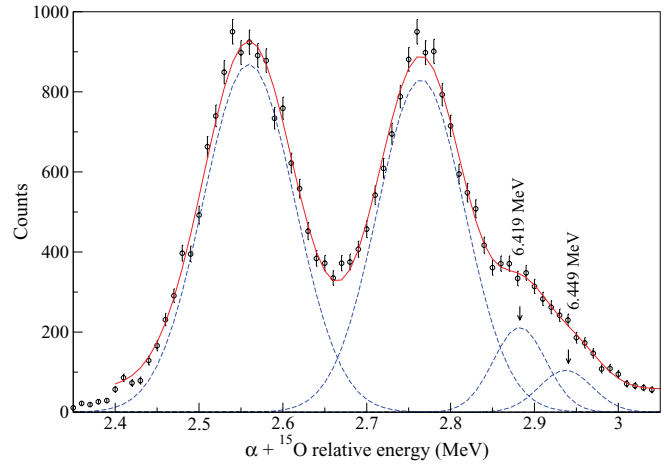

FIG. 10. (Color online) Relative energy spectrum for $\alpha + {}^{15}$O around $E_x = 6289$ keV, showing the fit for the 6419- and 6449-keV states in ^{19}Ne used to constrain the width of the 6449-keV state.

TABLE VI. The asymptotic normalization coefficients for $^{18}\mathrm{F} + p \rightarrow {}^{19}\mathrm{Ne}$ populating the subthreshold 6829-keV state. The numbers in parentheses are the statistical errors.

^{19}F		^{19}Ne (6289 keV)
E_x (keV)	J^π	C_p^2 (fm^{-1})
6497 6528	$3/2^+$	3479(92)
6255	$1/2^+$	6972(183)

where C_{sp} is the asymptotic normalization coefficient for the single-particle wave function. For the 6289-keV state, we find $C_{\mathrm{sp}}^2 = 1.53 \times 10^4$ fm^{-1}. The asymptotic normalization coefficients for the subthreshold 6289-keV state using the spins of its likely mirror states are shown in Table VI.

A 20% uncertainty is estimated for the proton width and asymptotic normalization coefficient. This systematic uncertainty has very little contribution from the binding potential, which affects both the calculated spectroscopic factor and single-particle width, but in opposite directions, with the result that proton width shows very little sensitivity to the details of the binding potential. The same is true for the asymptotic normalization coefficient. The overall systematic error in the proton width and asymptotic normalization coefficient essentially comes from the other optical potentials in the calculation.

C. Suggested isospin mirror levels in ^{19}F and ^{19}Ne

The assignment of spin and parity for some of the levels in ^{19}Ne important for the $^{18}\mathrm{F}(p,\alpha)$ reaction are taken from their putative mirror states in ^{19}F. The validity of estimating ^{19}Ne widths using mirror symmetry and widths from ^{19}F is not very certain. A comparison of the (d,n) and (d,p) data has provided considerable insight into the ^{19}F-^{19}Ne mirror symmetry for some of the levels observed in our experiment. The suggested pairs of states are listed in Table VII based on the $^{18}\mathrm{F}(d,p)^{19}\mathrm{F}$ and $^{18}\mathrm{F}(d,n)^{19}\mathrm{Ne}$ spectra in Figs. 8 and 9 and the DWBA analysis of the angular distribution extracted for the states in ^{19}F and ^{19}Ne.

The ^{19}F (6331) $\Leftrightarrow$ ^{19}Ne (6089) states are suggested as a possible mirror pair; both are populated via transfer to the $1d_{5/2}$ orbital in the same proportion with their mirror reaction and their angular distributions are identical. It is difficult to establish the mirror pair between the ^{19}Ne (6289) and the three likely mirror states in ^{19}F. This is partly due to two possible J^π values ($1/2^+$ or $3/2^+$) the state can have. Any of the three likely mirror states is a good candidate. In addition, the ^{19}F (6787) $\Leftrightarrow$ ^{19}Ne (6741) states are also suggested as a possible mirror pair. This analog connection is made as a result of both states being populated via a pure $\ell = 1$ transfer in the same proportion. Their extracted angular distributions are essentially identical. Utku *et al.* [37] also suggested the same mirror correspondence for the $1/2^-$ states. The analog of ^{19}Ne (7076 keV) is believed to be located in ^{19}F near 7300 keV [13]. The 7300-keV group in ^{19}F is composed of two unresolved states at 7262 and 7364 keV observed in this experiment. It is not very clear from our measurement which of the two levels is the analog state for ^{19}Ne (7076).

TABLE VII. Orbital momentum transfer and spectroscopic factor of the suggested mirror levels in ^{19}F and ^{19}Ne. The numbers in parentheses are the statistical errors.

^{19}F			^{19}Ne		
E_x (keV)	ℓ	$(2J+1)S_n$	E_x (MeV)	ℓ	$(2J+1)S_p$
6331	2	1.95(3)	6089	2	2.36(3)
6255/6497/6528	0	0.64(2)	6289	0	0.92(3)
6787	1	0.37(2)	6741	1	0.50(2)
7262/7364	0	0.67(2)	7076	0	1.47(5)

V. SUMMARY

The present study reports the proton-transfer and neutron-transfer reaction measurements on ^{18}F with radioactive beams. The technique of reconstructing the relative energy and light ejectile neutron (or proton) angle from the detected breakup products appears promising for future radioactive ion beam measurements. The quality of the spectroscopic data obtained can rival stable beam measurements and provide the precision necessary for astrophysical and nuclear structure applications away from stability.

The levels observed in ^{19}F appear to correspond to previously known states, and DWBA analysis of their angular distributions are consistent with known J^π assignments. The spectroscopic factors determined for these states agree reasonably well with the results of previous measurements.

The angular distributions extracted for levels in ^{19}Ne at $E_x = 6741$ and 7076 keV support their known $J^\pi = 3/2^-$ and $3/2^+$ assignments, respectively. The present measurements provide direct determination of the spectroscopic strengths of the controversial 8- and 38-keV resonances and provide constraints on the spin and parity values of these resonances. In this work, it is also shown that the $\ell = 0$ strength in ^{19}Ne around the proton threshold, previously thought to be concentrated in a state above the proton threshold, appears to be concentrated in the proton-bound 6289-keV state. The impact of these new result on the $^{18}\mathrm{F}(p,\alpha)^{15}\mathrm{O}$ reaction rate calculation and astrophysical consequences are presented in Ref. [20].

ACKNOWLEDGMENTS

We wish to acknowledge with thanks the technical and operations staff of HRIBF ORNL for their sense of commitment and hard work in making this experiment possible. This work was supported in part by the US Department of Energy under Grant Nos. DE-FG02-88ER40387 (OU), DE-FG02-93ER40789 (CSM), DE-FG02-96ER40990, DE-FG02-96ER40955 (TTU), and DE-FG52-08NA28552 (Rutgers) and by the NSF (Rutgers).

APPENDIX

The nature of the particle emission resulting from the decay $B \to C + c$ following the reaction $A(a, b)B$ is discussed in Sec. 10.7.4 of Satchler [38]. The double differential cross section for detecting b and c is given by Satchler, Eq. (10.126):

$$\frac{d^2\sigma}{d\Omega_b d\Omega_c} = \frac{d\sigma}{d\Omega_b}\frac{W}{4\pi}, \tag{A1}$$

where the branching-ratio factor Γ_c/Γ has been suppressed. The angular correlation function W is given by Satchler Eqs. (10.127) and (10.130) as

$$W = \sum_{kq} t_{kq}(I_B)\, R_k\, C^*_{kq}, \tag{A2}$$

where I_B and $t_{kq}(I_B)$ are the spin and polarization tensor of the nucleus B, R_k are the real radiation parameters, and C_{kq} are related to the spherical harmonics by

$$C_{kq} = \left[\frac{4\pi}{2k+1}\right]^{1/2} Y_{kq}. \tag{A3}$$

Following the convention used by FRESCO [30], we choose the z axis to be along the incident beam. We then have $t_{kq}(I_B) = t_{kq}(\theta_B)$ and $C_{kq} = C_{kq}(\theta_c, \phi_c)$, where $\theta_B = \pi - \theta_b$ and θ_c are the usual polar angles in the c.m. system and ϕ_c is the azimuthal angle between particles b and c.

The particle radiation parameters R_k are discussed in Sec. 10.7.4.2 of Satchler. Assuming that $B \to C + c$ occurs with a single orbital angular momentum L and channel spin S, we have

$$R_k = (2I_B+1)^{1/2}(2L+1)(-1)^{k+S-I_B}\langle LL00|k0\rangle \times W(LLI_BI_B;kS), \tag{A4}$$

where $\langle LL00|k0\rangle$ is a Clebsch-Gordon coefficient and $W(LLI_BI_B;kS)$ is a Racah coefficient. Parity conservation implies that k must be even. For the case of $^{19}\mathrm{Ne}^* \to {}^{15}\mathrm{O}(1/2^-) + \alpha(0^+)$ $S = \frac{1}{2}$ and L are uniquely determined for a given J^π state in ^{19}Ne. For the general case, relative partial width amplitudes for the decay $B \to C + c$ must be specified.

The polarization tensor $t_{kq}(I_B)$ describes the polarization of the final nucleus B; the precise definition is given in Secs. 10.3.2 and 10.3.3 of Satchler. The polarization tensors can be calculated with FRESCO by noting that the FRESCO scattering amplitudes $f_{m'M':mM}$ are equivalent to Satchler's transition matrix elements $T_{\beta\alpha}$ defined by his Eq. (9.2). Satchler's Eq. (10.32) reads

$$t_{kq}(I_B) = \frac{\mathrm{tr}[\boldsymbol{T}\boldsymbol{T}^\dagger\tau_{kq}(I_B)]}{\mathrm{tr}[\boldsymbol{T}\boldsymbol{T}^\dagger]}. \tag{A5}$$

In the notation of Thompson (analogous to Eq. (3.33) of Ref. [30]) this formula becomes

$$t_{kq}(I_B) = \frac{\mathrm{tr}[\boldsymbol{f}\boldsymbol{f}^\dagger\tau_{kq}(I_B)]}{\mathrm{tr}[\boldsymbol{f}\boldsymbol{f}^\dagger]} = \sqrt{2k+1}\,\frac{\sum_{m'M'mM} f_{m'M':mM}(\theta)^* f_{m'M'':mM}(\theta)\langle I_BM'kq|I_BM''\rangle}{\sum_{m'M'mM}|f_{m'M':mM}(\theta)|^2}, \tag{A6}$$

where $M'' = M' + q$ is required for the Clebcsh-Gordon coefficient to be nonzero. Also note that the differential cross section is given by

$$\frac{d\sigma}{d\Omega_b} = \frac{1}{(2I_A+1)(2I_a+1)}\sum_{m'M'mM}|f_{m'M':mM}(\theta)|^2. \tag{A7}$$

The above equations can be used to calculate the angular correlation using the scattering amplitudes output by FRESCO.

[1] A. Coc, M. Hernanz, J. José, and J.-P. Thibaud, Astron. Astrophys. **357**, 561 (2000).
[2] H. T. Fortune, A. Lacaze, and R. Sherr, Phys. Rev. C **82**, 034312 (2010).
[3] H. T. Fortune and R. Sherr, Phys. Rev. C **73**, 024302 (2006).
[4] H. T. Fortune and R. Sherr, Phys. Rev. C **61**, 024313 (2000).
[5] R. Coszach *et al.*, Phys. Lett. B **353**, 184 (1995).
[6] Y. M. Butt, J. W. Hammer, M. Jaeger, R. Kunz, A. Mayer, P. D. Parker, R. Schreiter, and G. Staudt, Phys. Rev. C **58**, R10 (1998).
[7] A. S. J. Murphy *et al.*, Phys. Rev. C **79**, 058801 (2009).
[8] D. W. Visser, J. A. Caggiano, R. Lewis, W. B. Handler, A. Parikh, and P. D. Parker, Phys. Rev. C **69**, 048801 (2004).
[9] D. W. Bardayan, J. C. Blackmon, J. Gomez del Campo, R. L. Kozub, J. F. Liang, Z. Ma, L. Sahin, D. Shapira, and M. S. Smith, Phys. Rev. C **70**, 015804 (2004).
[10] J.-S. Graulich *et al.*, Phys. Rev. C **63**, 011302 (2000).
[11] D. W. Bardayan *et al.*, Phys. Rev. Lett. **89**, 262501 (2002).
[12] R. L. Kozub *et al.*, Phys. Rev. C **73**, 044307 (2006).
[13] C. D. Nesaraja, N. Shu, D. W. Bardayan, J. C. Blackmon, Y. S. Chen, R. L. Kozub, and M. S. Smith, Phys. Rev. C **75**, 055809 (2007).
[14] M. J. Hornish, C. R. Brune, S. M. Grimes, M. H. Hadizadeh, T. N. Massey, A. V. Voinov, J. E. O'Donnell, A. Adekola, C. Matei, and Z. Heinen, in *Proceedings of the International Symposium on Nuclear Astrophysics—Nuclear in Cosmos IX, Geneva, Switzerland, 25–30 June 2006*, PoS (**NIC-IX**) 119 (2006).
[15] R. L. Kozub *et al.*, Phys. Rev. C **71**, R032801 (2005).
[16] H. Y. Lee *et al.*, Phys. Rev. C **81**, 015802 (2010).
[17] L. Gaudefroy *et al.*, Phys. Rev. C **78**, 034307 (2008).
[18] A. Obertelli *et al.*, Phys. Rev. C **74**, 064305 (2006).
[19] J. S. Thomas *et al.*, Phys. Rev. C **71**, 021302 (2005).
[20] A. S. Adekola *et al.*, Phys. Rev. C **83**, 052801(R) (2011).
[21] J. R. Beene, D. W. Bardayan, A. G. Uribarri, C. J. Gross, K. L. Jones, J. F. Liang, W. Nazarewicz, D. W. Stracener, B. A. Tatum, and R. L. Varner, J. Phys. G **38**, 024002 (2011).

[22] G. D. Alton, G. D. Mills, and J. Dellwo, Rev. Sci. Instrum. **65**, 2006 (1994).
[23] A. S. Adekola, Ph.D. thesis, Ohio University, 2008.
[24] MINUIT—Function Minimization and Error Analysis, CERN Program Library Long Writeup D506 (1994).
[25] N. de Séréville *et al*., Phys. Rev. C **67**, 052801 (2003).
[26] N. de Séréville, E. Berthoumieux, and A. Coc, Nucl. Phys. A **758**, 745c (2005).
[27] D. R. Tilley, H. R. Weller, C. M. Cheves, and R. M. Chasteler, Nucl. Phys. A **595**, 1 (1995).
[28] N. de Séréville *et al*., Nucl. Phys. A **718**, 259c (2003).
[29] P. D. Kunz, program DWUCK4 (unpublished).
[30] I. J. Thompson, Comput. Phys. Commun. **7**, 167 (1988).
[31] A. W. Barrows Jr., F. Gabbard, and J. L. Weil, Phys. Rev. **161**, 928 (1967).
[32] C. M. Perey and F. G. Perey, At. Data Nucl. Data Tables **17**, 1 (1976).
[33] C. M. Vincent and H. T. Fortune, Phys. Rev. C **7**, 865 (1973).
[34] J. P. Schiffer, Nucl. Phys. A **46**, 246 (1963).
[35] D. W. Bardayan *et al*., Phys. Rev. C **63**, 065802 (2001).
[36] M. Dufour and P. Descouvemont, Nucl. Phys. A **785**, 381 (2007).
[37] S. Utku *et al*., Phys. Rev. C **57**, 2731 (1998).
[38] G. R. Satchler, *Direct Nuclear Reactions* (Clarendon, Oxford, 1983).